Nanoscale

# One-step template-free synthesis of 3D functionalized flower-like boron nitride nanosheets for NH3 and CO2 adsorption



| | |
|---|---|
| Journal: | *Nanoscale* |
| Manuscript ID | NR-ART-03-2018-002074.R1 |
| Article Type: | Paper |
| Date Submitted by the Author: | 12-May-2018 |
| Complete List of Authors: | Chen, Yang; Deakin University, Institute for Frontier Materials<br>Wang, Jinfeng; Deakin University School of Life and Environmental Sciences,<br>Chen, Ying; Deakin University,<br>Liu, Dan; Deakin University, Institute for Frontier Materials<br>Huang, Shaoming; Wenzhou University, Nanomaterials and Chemistry Key Laboratory<br>Lei, Weiwei; Deakin University, Institute for Frontier Materials |
| | |

Journal Name

ARTICLE

# One-step template-free synthesis of 3D functionalized flower-like boron nitride nanosheets for $NH_3$ and $CO_2$ adsorption

Received 00th January 20xx,
Accepted 00th January 20xx

DOI: 10.1039/x0xx00000x

www.rsc.org/

Chen Yang,[a] Jinfeng Wang,[a] Ying Chen,*[a] Dan Liu,[a] Shaoming Huang,[b] and Weiwei Lei*[a]

3D functionalized flower-like boron nitride nanosheets (FBNNSs) were synthesized by a novel template-free method "cylinder compressing". Due to the high surface area (1114 $m^2/g$), pore volume (0.7 $cm^3/g$), hierarchical pore distributions and abundant edged groups (-OH and -$NH_2$), 3D functionalized FBNNSs displayed the excellent $NH_3$ and $CO_2$ adsorption up to 91 mg/g and 37.9 cc/g (74.4 mg/g) at 1 bar, respectively. Moreover, the reusable performance of gas adsorption was remained for 10 cycles, indicating the stable structure of FBNNSs. In addition, the adsorption mechanism was mainly explained by Lewis acid/base interaction, weak van der Waals interaction and H-bonds. The combination of enhanced adsorption capacity, excellent regenerability, extraordinary chemical and thermal stability made 3D FBNNSs possessing a huge potential for the implementation of practical $NH_3$ and $CO_2$ capture.

## 1. Introduction

$NH_3$ and $CO_2$, as typical alkaline and acidic gases discharged from extensive industrial emission and the consumption of fossil fuels, have arisen the hazard of human beings' health.[1-2] Therefore, the effective management of reducing the concentration of $NH_3$ and $CO_2$ in air is of colossal research interest as a sustainable energy supply and remediation of global climate change. In contrast with the traditional method of aqueous adsorption, the exploration and preparation of novel and high efficiency solid sorbent materials are considered as the environmentally friendly and economic ways due to the low corrosiveness, no volatility and reusable ability. Various solid adsorbents have been proposed as alternatives for harmful gases removal, including zeolite-based composites,[3-5] activated or porous carbon,[6-10] porous polymers[11-12] and metal organic frameworks.[13-16] However, they face the drawbacks of complex fabrication process, low adsorption capacity, unsatisfactory regeneration and unstability under harsh environment, which restrict the practical application. Consequently, the ideal harmful gases sorbents should endow several outstanding superiorities and conditions including facile preparation with large-scale and low cost, high adsorption capacity, ultra-stable performance as well as excellent regenerability for easy harmful gases capture/release.

Boron nitride nanosheets (BNNSs), with the structural analogue of graphene, have been regarded as one of typical two-dimensional (2D) materials for scientific research and commercial demand. Due to unique polar B-N covalent bonds, BNNSs have possessed a number of fascinating properties including strong oxidation resistance, chemical inertness, electrical insulation and high thermal conductivity.[17] Such outstanding properties make them promising in extensively applications such as water cleaning,[18-22] $H_2$ storage[23], anticancer drug delivery,[24-25] and catalyst supports[26], as well as endow BNNSs a huge potential as a promising gas adsorbent.

However, there are only few reports on BN materials for $CO_2$ capture and no report on BN materials for $NH_3$ adsorption.[27] The most significant challenge of applying BNNSs as gas adsorbent is the weak interactions between BN nanosheets and $CO_2$ and $NH_3$ due to the vacant p-like orbitals of the B atoms in BNNSs materials. To improve the adsorption capacity of $CO_2$ and $NH_3$ on BNNSs surface, porous BNNSs with the large surface, huge pore volume and abundant pore sizes distributions will be greatly increased the physical adsorption. In addition, functionalized BNNSs such as various acidic groups (sulfonic, hydroxyl, carboxylic and epoxide groups) or basic groups (-$NH_2$ and –NH-) as adsorption sites will also be enhanced the adsorption capacity of $CO_2$ and $NH_3$ ascribed to the strengthened chemical interaction between functional groups and gas molecules. For example, Huang et al. confirmed that amine functionalized BN with the polyethyleneimine (PEI) can improve the $CO_2$ adsorption ability.[28] Therefore, the integration of individual BNNSs into three-dimensional (3D) porous structure with functional groups is considered to be one of most effective strategies to significantly enhance their gas adsorption capacity. Currently, many novel 3D BN assemblies have been fabricated by a various techniques. Among them, template-free synthesis or dynamic template approach is the mainstream and green

[a] Institute for Frontier Materials, Deakin University, Locked Bag 2000, Geelong, Victoria 3220, Australia.
E-mail: ian.chen@deakin.edu.au; weiwei.lei@deakin.edu.au
[b] Nanomaterials & Chemistry Key Laboratory, Wenzhou University, Wenzhou, P. R. China.

preparation method without extra chemicals as nanostructure-directed agents and the post-purification process.[29-31] For instance, Liu et al. prepared 3D novel BN spheres with a specific surface area of 196.5 $m^2/g$ as versatile sorbent.[32] Xue et al. demonstrated a two-step template-free reaction involving self-bubbling solidification of precursors and pyrolysis process for constructing 3D porous BN architectures materials with higher specific surface areas over 1400 $m^2/g$.[30] Weng et al. reported a highly porous 3D BN sponge with ultrahigh surface areas up to 1900 $m^2/g$ for $H_2$ storage.[31] However, 3D functionalized BN network from nanosheets with highly porous nanostructures in the application of gas adsorption have not been reported.

Here, we report on the development of hydroxyl (-OH)/amino (-$NH_2$) co-functionalized 3D BNNSs with porous textures and controlled flower-like morphology via a novel one-step template-free "cylinder compressing" method. The resultant 3D flower-like boron nitride (FBNNSs) were effectively employed for gas adsorption due to its wide range porosities from micro- to meso-pores and richly functional groups. Additionally, it is first time to experimentally exhibit the outstanding $NH_3$ adsorption around 91 mg/g. Furthermore, 3D FBNNSs present the best $CO_2$ adsorption around 37.9 cc/g (74.4 mg/g) at 273 K and 19.2 cc/g (37.7 mg/g) at 298 K, respectively. Owing to the good oxidation resistance and notable chemical inertness, they could be easily recovered and exhibited excellent recycling stability up to 10 cycles for $NH_3$ and $CO_2$.

## 2. Experimental

**2.1 Materials.** Boron oxide ($B_2O_3$), guanidine hydrochloride ($CH_5N_3$·HCl) and methanol ($CH_3OH$) were purchased from Sigma-Aldrich without extra purification.

**2.2 Synthesis of 3D FBNNSs.** Boron oxide (0.56 g, 99.98%) and guanidine hydrochloride (3.95 g, 98%) were mixed in 10 mL methanol and stirred for 24 h to form a homogeneous solution. As-dried precursor mixture (1.5 g) in air presented crystalline powders and was mechanically compressed to a cylinder (radius: 5 mm; height: 15 mm) using 3 tons force around 5 min. The cylinder precursor was heated up to 1050 ℃ with a heating rate of 1.5 ℃/min and kept this temperature for 2 h under $N_2$ atmosphere at a rate of one bubble per second.

**2.3 Characterization.** The specific flower-like nanostructures were carried out by scanning electron microscopy (SEM, Zeiss Supra 55 VP) and transmission electron microscopy (TEM, JEOL 2100 LaB6 instrument, 200 kV). The chemical constituents were characterized by X-ray diffraction (XRD, Panalytical X'Pert PRO diffraction system using Cu $K_\alpha$ radiation), Raman spectroscopy (Renishaw confocal micro-Raman spectrometers, 633 nm lasers) and Fourier transform infrared spectroscopy (FTIR, Bruker Vertex 70) spectra. X-ray photoelectron spectroscopy (XPS, ESCALAB 250 instrument) was performed to analyse the information of surface composition of 3D FBNNSs. $N_2$ physical adsorption and desorption were measured by Quantachrome Autosorb iQ3 instrument at 77 K. All samples were degassed at 120 ℃ for 12 h under vacuum condition and employed Brunauer-Emmett-Teller equation to calculate the specific surface area by collecting the adsorption data at the relative pressure (P/P0) from 0.05-0.3. Quenched solid density functional theory (QSDFT) method was used for the analysis of pore size distribution of 3D FBNNSs.

**2.4 $NH_3$ Adsorption Measurement.** To evaluate the $NH_3$ capture performance, the dynamic adsorption method (Miran 1A Infra-red Spectrometer) was employed. Briefly, 3D FBNNSs were placed in the test chamber with the volume of 8 L. A certain volume of $NH_3$ was injected into the pump and the initial concentration was controlled around 0.15 mg/L. The odour quickly went through the adsorption chamber and then circulated in the sealed gas detection system. The Miran 1A Infra-red Spectrometer was used to reflect the concentration change of $NH_3$ by detecting the signal change of N-H bonds in $NH_3$ molecules. All adsorption equilibrium data were collected for 22 h at room temperature and 1 atm. Furthermore, the saturated materials could be degassed for reuse by simple heating to 80 ℃ in vacuum oven for 3 h and maintain such high performance characteristics for 5 times

**2.5 Calculation of $NH_3$ adsorption capacity.** In order to display the outstanding capture ability from 3D FBNNSs, the equation was defined as follow:

$$C=[8L*(C_e-C_o)]/m \quad (1)$$

Where C stand for the removal capacity of $NH_3$, while $C_e$ and $C_0$ reflected the initial and equilibrium concentrations of $NH_3$, respectively. The m was the quantity of 3D FBNNSs.

**2.6 $CO_2$ Adsorption Measurement.** The $CO_2$ adsorption tests were run on Quantachrome Autosorb iQ3 instrument from 0-1 bar at 273 K and 298 K, respectively. Before $CO_2$ adsorption, all samples were degassed at 250 ℃ for 12 h under vacuum condition.

## 3. Results and discussion

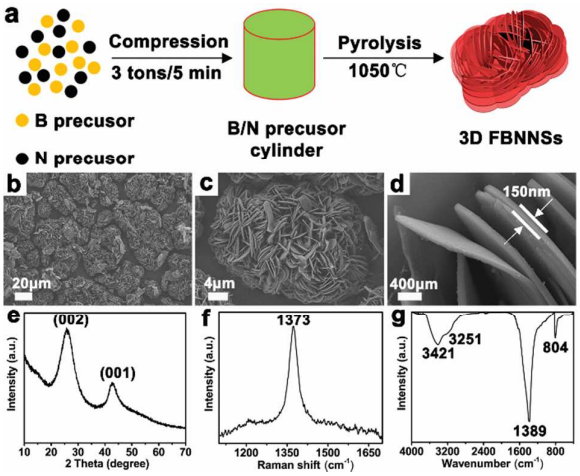

**Figure 1.** (a) Schematic procedures of 3D FBNNSs preparation. (b) Low-magnification and (c and d) high-magnification SEM image; (e) Typical XRD pattern, (f) Raman spectra and (g) FTIR spectra of 3D FBNNSs.

**3.1 Characterization of 3D Nanostructure and Chemical Bonds.** As Figure 1a depicted, in a typical synthesis boron oxide and guanidine hydrochloride as corresponding B and N sources were firstly compressed into B/N precursor cylinder. Secondly, 3D functionalized FBNNSs could be acquired via the pyrolysis process under the conditions of low heating rate and $N_2$ flow. SEM images (Figure 1b and c) indicated that resultant products showed unique 3D flower-like morphology consisting of tightly packed nanosheets in well-ordered fashion with a size approximately from 10 μm to 100 μm, while the thickness was around 150 nm as showed in Figure 1d. Figure 1e indicated that the peaks located at 25.7° and 42.5° in XRD pattern were assigned to (002) and (001) lattice planes from h-BN, respectively.[33-34] Raman spectroscopy was used to further analyse the structure of BN crystalline in Figure 1f. Compared with the $E_{2g}$ vibration mode placed around at 1366 $cm^{-1}$ for bulk h-BN, as-obtained Raman signature was red shifted to 1373 $cm^{-1}$ due to the interaction of enlarged (002) BN interlayers.[35] FTIR exhibited the distinct features of BN materials that peaks at 1389 $cm^{-1}$ and 804 $cm^{-1}$ verified the existence of in-plane $sp^2$-bonded B-N stretching mode ($E_{1u}$) and out-of-plane $sp^2$-bonded B-N-B bending mode ($A_{2u}$) as shown in Figure 1g. Two more peaks at 3421 and 3251 $cm^{-1}$ derived from -OH and -$NH_2$ groups and implied the "cylinder compressing" synthesis strategy involved the efficient covalent chemical functionalization.[34, 36] This effectively functionalization of –OH/ –$NH_2$ in 3D FBNNSs could be explained by structural and surface defects.[37] Due to the unique preparation, highly porous 3D FBNNSs endowed numerous vacancy defects and structural dislocations to expose more activated edge sites to capture –OH/-$NH_2$ groups. Meanwhile, a large amount of O- and N- sources from $B_2O_3$ and $CH_5N_3$·HCl at high reaction temperature (1050 ℃) further contributed to the formation of –OH/ –$NH_2$ functionalization, which was in accordance with previous results that –OH/–$NH_2$ groups could be functionalized to BN using various precursors during the pyrolysis process at high temperature (1000~1300 ℃).[38-40] Therefore, we suggested that the growth mechanism combined the nucleation and self-assembly processes similar to the previous report of vertical BNNSs fabrication on silicon substrate.[41] Initially, the precursor vapor was released slowly from the surface of the cylinder ascribed to the low heating rate and tightly compressed solid phase. Upon the nucleation started in gas phase, numerous porous BNNSs were triggered to grow homogeneously and then assembled into 3D flower-like morphology simultaneously accompanying with –OH/ –$NH_2$ functionalization. Consequently, the low heating rate, low $N_2$ flow and constricted solid phase of precursors acted as the keys to 3D FBNNSs assembly process.

**3.2 Porous Surface Analysis of 3D FBNNSs.** To evaluate the porosity of 3D FBNNSs, TEM images (Figure 2a and b) revealed the sponge-like surface and dislocation nanostructures, which firmly proved the existence of porous textures. As well-known, the parallel (002) lattice fringes of h-BN materials was of 0.33-0.34 nm.[35, 42] However, high-resolution TEM image (Figure 2b) illustrated that 3D FBNNSs owned the slit-shaped pores arisen from enlarged

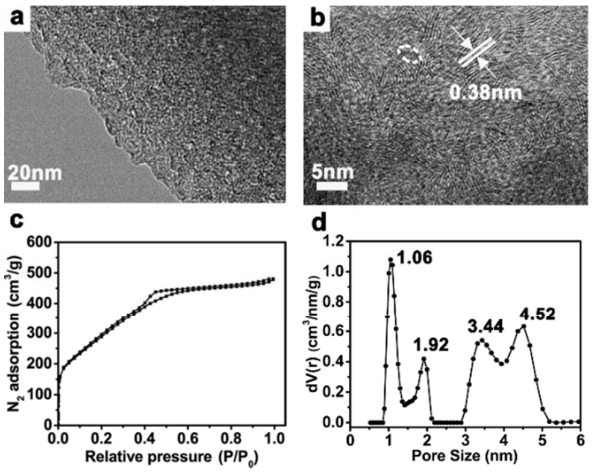


**Figure 2.** (a) TEM and (b) HRTEM images of 3D FBNNSs; (c) $N_2$ adsorption-desorption isotherm and (d) pore size distribution.

interspacing between adjacent fringes (0.38 nm) and the pores over 1 nm surrounded via distorted layers as similar as the previous research proposed.[30-31] Meanwhile, $N_2$ adsorption-desorption isotherm (Figure 2c) provided a high surface area about 1114 $m^2$/g and high pore volume of 0.7 $cm^3$/g. According to IUPAC classification, the shape of type Ⅰ isotherm curve and H4-type hysteresis loops further demonstrated the small meso- and slit-like porosity in 3D FBNNSs in accordance with TEM results and the red-shifted Raman signal.[36] Additionally, the hierarchical pore distributions were displayed in Figure 2d and proved that 3D FBNNSs mainly consisted of micro-pores (1.06 and 1.92 nm) and small meso-pores (3.44 and 4.52 nm) via QSDFT method in consideration of the heterogeneous and rough surface nanostructure.[30] Consequently, the physically mesopores structure of 3D functionalized FBNNSs was expected to be a novel $NH_3$ and $CO_2$ capture due to the efficient contact surface area and more adsorption sites.

**3.3 $NH_3$ and $CO_2$ Capture of 3D FBNNSs.** To investigate the gas adsorption capacity of 3D functionalized FBNNSs, we selected two different gases, alkaline ($NH_3$) and acidic ($CO_2$), and then measured the gas adsorption performance. Figure 3a showed the real-time change of $NH_3$ concentration on h-BN and 3D functionalized FBNNSs at room temperature and 1 bar. As could be seen that, the $NH_3$ concentration decreased fast in initial 2 h due to the instantaneous availability of large surface area and active adsorption sites. The adsorption was almost completed after 22 h with an adsorption capacity of 91 mg/g according to the calculation equation (1). This adsorption capacity was much higher than recent refined adsorbents including graphene/nanoporous carbon (<21.8 mg/g),[43] $Fe_3C$-

derived carbon/Fe nanoparticles (32 mg/g),[44] activated Alumina (<53 mg/g)[2]. When commercial h-BN was tested under the same conditions, the adsorbance was reduced by 61 mg/g, indicating essential performance enhancement from highly porosity and richly functional groups. More importantly, almost all of the captured $NH_3$ could be released simply by heating at 80 ℃. The regeneration behaviour of 3D FBNNSs upon $NH_3$ adsorption for

**Figure 3.** (a) $NH_3$ adsorption of h-BN and 3D FBNNSs at first

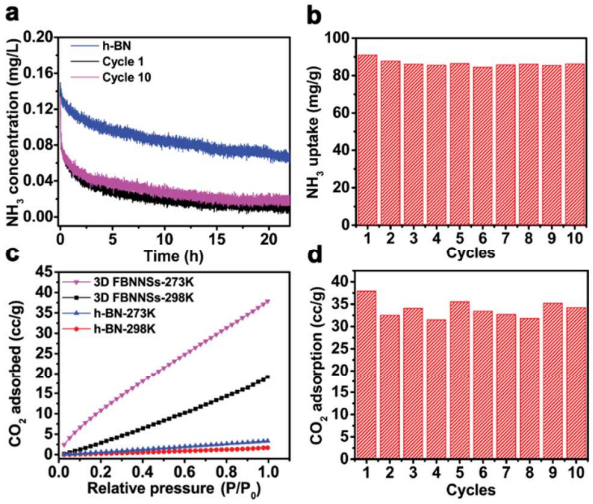


and tenth cycle; (b) 10 cycling adsorption. (c) $CO_2$ adsorption isotherms of h-BN and 3D FBNNSs at 273 K and 298 K from 0-1 bar; (d) reusable adsorption of 3D FBNNSs at 273 K.

10 cycles test. As shown in Figure 3a and b, the removal capacity of $NH_3$ still remain around 86.2 mg/g after 10$^{th}$ cycle, suggesting a good recycling stability of the sample as the gas cleaning adsorbent. Another significant feature of 3D functionalized FBNNSs was their strong $CO_2$ adsorption capability at 273 K and 298 K from 0 to 1 bar in Figure 3c. The 3D functionalized FBNNSs displayed an excellent $CO_2$ capture ability of 37.9 cc/g (74.4 mg/g) at 273 K and 1 bar. In addition, the $CO_2$ adsorption capacity still could be reached to 19.2 cc/g (37.7 mg/g) at higher temperature condition of 298 K. As shown in Figure 3c, it disclosed clearly that commercial h-BN showed a negligible removal capacity (~3.3 cc/g (6.5 mg/g) at 273 K and 1.7 cc/g (3.4 mg/g) at 298 K). Furthermore, the maximum $CO_2$ adsorption of 3D functionalized FBNNSs was appreciably twice higher than recently reported BNNSs, as summarized in Table 1.[27-28] Additionally, Figure 3d exhibited the stable reusability of the 3D functionalized FBNNSs for $CO_2$ capture up to 10 cycles contributed to the intrinsic chemical inertness and thermal stability of BN.[45] These excellent performance could be advantageous for arresting $CO_2$ from flue gas. As we known that the main challenge in capturing $CO_2$ from flue gas was the low

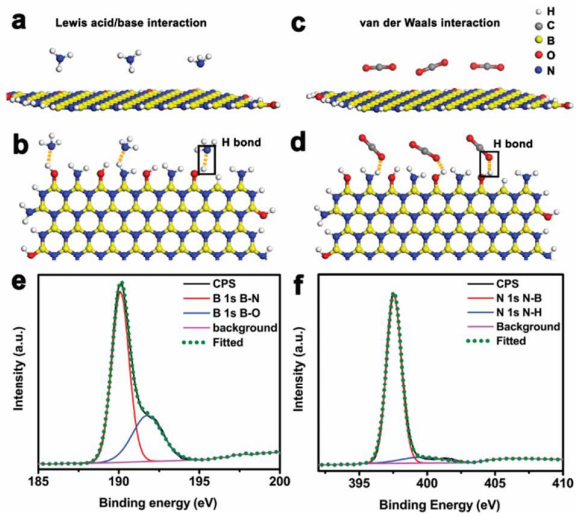


**Figure 4.** $NH_3$ and $CO_2$ adsorption of 3D FBNNSs: Plane-adsorption sites of (a) $NH_3$ and (c) $CO_2$; Edged groups adsorption sites of (b) $NH_3$ and (d) $CO_2$. XPS spectra of 3D FBNNSs: high-resolution core-level (e) B 1s and (f) N 1s.

$CO_2$ partial pressure, whereas the richly porosities and functional groups created sufficient active $CO_2$-adsorbing centres to grab the acidic guest molecules at 1 bar. Therefore, -OH/-$NH_2$ co-functionalized 3D FBNNSs owned the high double performance for $NH_3$ and $CO_2$ adsorption.

**3.4 Adsorption Mechanism of $NH_3$ and $CO_2$ on 3D FBNNSs.** Aiming to gain a better understanding of why the 3D functionalized FBNNSs possessed the enhanced $NH_3$ and $CO_2$ adsorption capacity, two aspects contributed to the aforementioned results. Firstly, this hierarchically porous structure was extremely advantageous for higher volume $NH_3$ and $CO_2$ adsorption application, since the mesopores would provide a low-resistant pathway for the diffusion of $NH_3$ and $CO_2$ molecules while the micropores would offer more adsorption sites for trapping $NH_3$ and $CO_2$. Secondly, functional groups were also benefit to promote the arrestment of $NH_3$ and $CO_2$. As shown in Figure 4a and b, $NH_3$ molecules preferred to be captured at in-plane of BNNSs and terminal -OH/-$NH_2$ groups.

**Table 1.** Summary of $NH_3$ and $CO_2$ adsorption at 1 bar in comparison to commercial h-BN and reported BN materials.

| Materials | $S_{BET}$ ($m^2$/g) | PV ($cm^3$/g) | $NH_3$ (mg/g, 298 K) | $CO_2$ (cc/g) | | | | Reference |
|---|---|---|---|---|---|---|---|---|
| | | | | 273 K | 298 K | 303 K | 348 K | |
| FBNNSs | 1114 | 0.7 | 91 | 37.9 | 19.2 | - | - | this work |
| h-BN | - | - | 61 | 3.3 | 1.7 | - | - | this work |
| BNNSs | <236 | - | - | <16 | <10 | - | - | [27] |

| | | | | | | | | |
|---|---|---|---|---|---|---|---|---|
| BN | 280 | 0.24 | - | - | - | 12.5 | 6.5 | [28] |
| PEI@BN | <36 | <0.09 | - | - | - | 31.8 | 69.9 | [28] |

Such good $NH_3$ adsorption performance not only belonged to typical physical adsorption behaviour involving $NH_3$ molecules embedment into pores and slits of 3D FBNNSs, but also the weak chemical adsorption behaviour explained via the theory of Lewis acid/base interaction and H bonds formation. Different from non-polar C-C bonds in graphene, the specific polarity property of B-N bonds originating from electronegativity difference endowed B and N atoms with the partial positive and negative charges, respectively. On the base of previous density functional theory (DFT) analysis, N atom in $NH_3$ molecule acted as nucleophilic species toward B atom in BNNS plane surface, while electrophilic behaviour existed between H atom in $NH_3$ molecule and N atom in BNNS surface (Figure 4a).[46-48] Moreover, H bonds were also formed among $NH_3$ molecules and -OH/-$NH_2$ edged groups as showed by dotted line in Figure 4b, further increasing $NH_3$ capture efficiency.[48] Additionally, $CO_2$ molecules also had a tendency to be adsorbed at in-plane and edged groups of BNNSs. Apart from the H-bonds between $CO_2$ and -OH/-$NH_2$ groups, the physical $CO_2$ capture on the in-plane of BNNSs predominately relied on weak van der Waals interaction with three different adsorption configures including at the top place of B or N atoms (t-B or N site), the bridge site of B-N bond and the hollow ring in hexagonal BN unit as similar to previous investigation of $CO_2$ adsorption on h-BN nanosheets and BN nanotubes by DFT calculations (Figure 4c and d).[49-51] Meanwhile, t-B and N sites were considered as the most stable capture configurations according to the calculation of binding energies. Specifically, when a $CO_2$ molecule was parallel to BNNSs and over at t-N site, the intersection existed between the projection of two C-O bond and B-N bond. While, the projection of linear $CO_2$ overlapped with the B–N bond and $CO_2$ molecules tilted a little angle to the BNNS surface.[50] Besides, the existence of lattice vacancies and defects was another adsorption sites for the arrestment of $CO_2$ molecules.[52] Therefore, the enrichment of porous nanostructure in plane and functional groups on edges increased the $NH_3$ and $CO_2$ capture ability. In order to estimate the respective contribution of gas capture capacity from the in-planes and on-edges of 3D FBNNSs, XPS spectra was carried out to collect the surface composition. As shown in the Figure 4e, the higher resolution core-level XPS result identified B 1s peak at ~190.1 eV and was fitted into B-N bonds at ~ 190.0 eV and B-OH at ~191.7 eV.[53] The peak at ~397.6 eV was classified to N 1s with the fitted peaks including N-B bonds (~397.5 eV) and N-H bonds (~399.7 eV).[54] The XPS analysis was not only in accordance with XRD results, but also further demonstrated that the contents of B-OH and –N-H groups from the edges of 3D FBNNSs were ~5.3% and ~4.2%, respectively. Therefore, the minor capture capacity of $NH_3$ or $CO_2$ was from the sites of edged groups (B-OH and N-H bonds) ascribed to the H-bonds, while the major contribution of $NH_3$ or $CO_2$ was adsorbed in the plane of FBNNSs due to Lewis acid/base interaction and van der Waals interaction respectively.[55] Consequently, both $NH_3$ and $CO_2$ were captured predominantly in plane of porous 3D FBNNSs.

## 4. Conclusions

In summary, we successfully propose a new synthesis strategy, “cylinder compressing” method, to produce morphology-controlled 3D functionalized flower-like BNNSs. Significantly, the 3D functionalized FBNNSs exhibits much improved $NH_3$ and $CO_2$ adsorption capacity in comparison with pristine h-BN. Due to their unique 3D structure with high specific surface area, high pore volume and hierarchical porosities, as well as the polar surface with edge-terminated groups (-OH and -$NH_2$) stemmed from the “lop-sided” densities feature of ionic B-N bonds. Furthermore, the $NH_3$ and $CO_2$ adsorption can be easily desorbed from 3D FBNNSs at a relatively moderated temperature and 3D FBNNSs demonstrate high stability capture/release cycles. Based on the results obtained in this work, it is concluded that 3D functionalized FBNNSs is an effective way to extend their application in the field of air cleaning.

## Conflicts of interest

There are no conflicts to declare.

## Acknowledgements

This work was financially supported by the Australian Research Council Discovery Program, the Australian Research Council Discovery Early Career Research Award scheme (DE150101617 and DE140100716) and Central Research Grant Scheme of Deakin University.

## Notes and references

1 Ullah, R.; Atilhan, M.; Diab, A.; Deniz, E.; Aparicio, S.; Yavuz, C. T. *Adsorption,* 2016**, *22***, 247-260.
2 Saha, D.; Deng, S. G. *J. Chem. Eng. Data,* 2010, ***55***, 5587-5593.
3 Su, F. S.; Lu, C. Y. *Energ. Environ. Sci.,* 2012**, *5***, 9021-9027.
4 Song, Z. N.; Huang, Y.; Wang, L.; Li, S. G.; Yu, M. *Chem. Commun.,* 2015, ***51***, 373-375.
5 Ding, W. J.; Klumpp, M.; Li, H.; Schygulla, U.; Pfeifer, P.; Schwieger, W.; Haas-Santo, K.; Dittmeyer, R. *J. Phys. Chem. C,* 2015, ***119***, 23478-23485.
6 Ding, S. M.; Dong, Q. L.; Hu, J. W.; Xiao, W. M.; Liu, X. H.; Liao, L. Q.; Zhang, N. *Chem. Commun.,* 2016, ***52***, 9757-9760.

7 Fu, N.; Wei, H. M.; Lin, H. L.; Li, L.; Ji, C. H.; Yu, N. B.; Chen, H. J.; Han, S.; Xiao, G. Y. *Acs. Appl. Mater. Inter.,* 2017, ***9***, 9955-9963.
8 Hong, S. M.; Choi, S. W.; Kim, S. H.; Lee, K. B. *Carbon,* 2016, ***99***, 354-360.
9 Tiwari, D.; Bhunia, H.; Bajpai, P. K. *Rsc Adv.,* 2016, ***6***, 111842-111855.
10 Wang, Y.; Zou, H. B.; Zeng, S. J.; Pan, Y.; Wang, R. W.; Wang, X.; Sun, Q. L.; Zhang, Z. T.; Qiu, S. L. *Chem. Commun.,* 2015, ***51***, 12423-12426.
11 Yang, X.; Yu, M.; Zhao, Y.; Zhang, C.; Wang, X. Y.; Jiang, J. X. *J. Mater. Chem. A,* 2014, ***2***, 15139-15145.
12 Liu, B.; Miao, H.; Pang, L. Y.; Hou, L.; Wang, Y. Y.; Shi, Q. Z. *Crystengcomm.,* 2012, ***14***, 2954-2958.
13 Zhang, Z. J.; Zhao, Y. G.; Gong, Q. H.; Li, Z.; Li, J. *Chem.Commun.,* 2013, ***49***, 653-661.
14 Majumder, M.; Sheath, P.; Mardel, J. I.; Harvey, T. G.; Thornton, A. W.; Gonzago, A.; Kennedy, D. F.; Madsen, I.; Taylor, J. W.; Turner, D. R.; Hill, M. R. *Chem. Mater.,* 2012, ***24***, 4647-4652.
15 Li, Y. W.; Yan, H.; Hu, T. L.; Ma, H. Y.; Li, D. C.; Wang, S. N.; Yao, Q. X.; Dou, J. M.; Xu, J.; Bu, X. H. *Chem. Commun.,* 2017, ***53***, 2394-2397.
16 Hu, X. L.; Liu, F. H.; Wang, H. N.; Qin, C.; Sun, C. Y.; Su, Z. M.; Liu, F. C. *J. Mater. Chem. A,* 2014, ***2***, 14827-14834.
17 Jiang, H. B.; Wang, Z. F.; Geng, H. Y.; Song, X. F.; Zeng, H. B.; Zhi, C. Y. *Acs Appl. Mater. Inter.,* 2017, ***9***, 10078-10084.
18 Lei, W. W.; Liu, D.; Chen, Y. *Adv. Mater. Interfaces,* 2015, ***2***, 1400529.
19 Lei, W. W.; Portehault, D.; Liu, D.; Qin, S.; Chen, Y. *Nat. Commun.,* 2013, ***4***, 1777.
20 Lian, G.; Zhang, X.; Si, H. B.; Wang, J.; Cui, D. L.; Wang, Q. L. *Acs Appl. Mater. Inter.,* 2013, ***5***, 12773-12778.
21 Wang, J.; Hao, J.; Liu, D.; Qin, S.; Chen, C.; Yang, C.; Liu, Y.; Yang, T.; Fan, Y.; Chen, Y. *Nanoscale,* 2017, **9**, 9787-9791.
22 Liu, D.; Lei, W. W.; Qin, S.; Klika, K. D.; Chen, Y. *Phys. Chem. Chem. Phys.,* 2016, ***18***, 84-88.
23 Lei, W. W.; Zhang, H.; Wu, Y.; Zhang, B.; Liu, D.; Qin, S.; Liu, Z. W.; Liu, L. M.; Ma, Y. M.; Chen, Y. *Nano Energy,* 2014, ***6***, 219-224.
24 Li, X.; Wang, X. P.; Zhang, J.; Hanagata, N.; Wang, X. B.; Weng, Q. H.; Ito, A.; Bando, Y.; Golberg, D. *Nat. Commun.,* 2017, ***8***, 13936.
25 Weng, Q. H.; Wang, B. J.; Wang, X. B.; Hanagata, N.; Li, X.; Liu, D. Q.; Wang, X.; Jiang, X. F.; Bando, Y.; Golberg, D. *Acs Nano,* 2014, ***8***, 6123-6130.
26 Liu, D. A.; Zhang, M. W.; Xie, W. J.; Sun, L.; Chen, Y.; Lei, W. W. *Appl. Catal. B-Environ.,* 2017, ***207***, 72-78.
27 Xiao, F.; Chen, Z.; Casillas, G.; Richardson, C.; Li, H.; Huang, Z. *Chem. Commun.,* 2016, ***52***, 3911-3914.
28 Huang, K.; Liang, L.; Chai, S.; Tumuluri, U.; Li, M.; Wu, Z.; Sumpter, B. G.; Dai, S. *J. Mater. Chem. A,* 2017, **5**, 16241-16248.
29 Liu, D.; Lei, W. W.; Qin, S.; Chen, Y. *Sci. Rep.,* 2014, ***4, 4453***.
30 Xue, Y. M.; Dai, P. C.; Jiang, X. F.; Wang, X. B.; Zhang, C.; Tang, D. M.; Weng, Q. H.; Wang, X.; Pakdel, A.; Tang, C. C.; Bando, Y.; Golberg, D. *J. Mater. Chem. A,* 2016, ***4***, 1469-1478.
31 Weng, Q. H.; Wang, X. B.; Bando, Y.; Golberg, D. *Adv. Energy. Mater.,* 2014, ***4, 1301525***.
32 Liu, F.; Yu, J.; Ji, X.; Qian, M. *Acs Appl. Mater. Inter.,* 2015, ***7***, 1824-1832.
33 Nazarov, A. S.; Demin, V. N.; Grayfer, E. D.; Bulavchenko, A. I.; Arymbaeva, A. T.; Shin, H. J.; Choi, J. Y.; Fedorov, V. E. *Chem-Asian J,* 2012, ***7***, 554-560.
34 Gao, R.; Yin, L. W.; Wang, C. X.; Qi, Y. X.; Lun, N.; Zhang, L. Y.; Liu, Y. X.; Kang, L.; Wang, X. F. *J. Phys. Chem. C,* 2009, ***113***, 15160-15165.
35 Weng, Q.; Wang, X.; Zhi, C.; Bando, Y.; Golberg, D. *ACS Nano,* 2013, ***7***, 1558-1565.
36 Li, J.; Xiao, X.; Xu, X. W.; Lin, J.; Huang, Y.; Xue, Y. M.; Jin, P.; Zou, J.; Tang, C. C. *Sci. Rep.,* 2013, ***3, 3208***.
37 Yu, J.; Hou, X.; Wang, M.; Fu, L.; Chen, Y.; Jiang, N.; Lin, C.-T.; Wang, Z. *Nanoscale,* **2018**. DOI: 10.1039/C8NR00651B
38 Li, J.; Xiao, X.; Xu, X. W.; Lin, J.; Huang, Y.; Xue, Y. M.; Jin, P.; Zou, J.; Tang, C. C. *Sci. Rep.,* **2013,** *3*, 3208. DOI: 10.1038/srep03208
39 Lei, W. W.; Portehault, D.; Liu, D.; Qin, S.; Chen, Y. *Nat. Commun.,* **2013,** *4*, 1777. DOI: 10.1038/ncomms2818
40 Dibandjo, P.; Bois, L.; Chassagneux, F.; Cornu, D.; Letoffe, J. M.; Toury, B.; Babonneau, F.; Miele, P. *Adv. Mater.,* **2005,** *17*, 571-574.
41 Pakdel, A.; Zhi, C.; Bando, Y.; Nakayama, T.; Golberg, D. *ACS Nano,* 2011, ***5***, 6507-6515.
42 Lin, Y.; Williams, T. V.; Connell, J. W. *J. Phys. Chem. Lett.,* 2010, ***1***, 277-283.
43 Corre, Y.; Seredych, M.; Bandosz, T. J. *Carbon,* 2013, ***55***, 176-184.
44 Mangarella, M. C.; Walton, K. S. *Carbon,* 2015, ***95***, 208-219.
45 Chen, S.; Li, P.; Xu, S.; Pan, X.; Fu, Q.; Bao, X. *J. Mater. Chem. A,* **2018,** *6*, 1832-1839.
46 Li, H.; Chen, Z.; Fang, X. L.; Tie, D. Y. *Superlattice Microst.,* 2015, ***88,*** 371-376.
47 Sundaram, R.; Scheiner, S.; Roy, A. K.; Kar, T. *Phys. Chem. Chem. Phys.,* 2015, ***17***, 3850-3866.
48 Li, Y. F.; Zhou, Z.; Zhao, J. *J. Chem. Phys.,* 2007, ***127***, *184705*.
49 Sun, Q.; Li, Z.; Searles, D. J.; Chen, Y.; Lu, G. Q.; Du, A. J. *J. Am. Chem. Soc.,* 2013, ***135***, 8246-8253.
50 Guo, H. Y.; Zhang, W. H.; Lu, N.; Zhuo, Z. W.; Zeng, X. C.; Wu, X. J.; Yang, J. L. *J. Phys. Chem. C.,* 2015, ***119***, 6912-6917.
51 Paura, E. N. C.; da Cunha, W. F.; Martins, J. B. L.; Silva, G. M. E.; Roncaratti, L. F.; Gargano, R. *Rsc Adv.,* 2014, ***4***, 28249-28258.
52 Paura, E. N. C.; da Cunha, W. F.; Roncaratti, L. F.; Martins, J. B. L.; Silva, G. M. E.; Gargano, R. *Rsc Adv.,* 2015, ***5***, 27412-27420.
53 Lee, D.; Lee, B.; Park, K. H.; Ryu, H. J.; Jeon, S.; Hong, S. H. *Nano Lett.,* **2015,** *15*, 1238-44.
54 Lei, W.; Mochalin, V. N.; Liu, D.; Qin, S.; Gogotsi, Y.; Chen, Y. *Nat. Commun.,* **2015,** *6*, 8849. DOI: 10.1038/ncomms9849
55 Lakhi, K. S.; Park, D.-H.; Singh, G.; Talapaneni, S. N.; Ravon, U.; Al-Bahily, K.; Vinu, A. *J. Mater. Chem. A,* **2017,** *5*, 16220-16230.

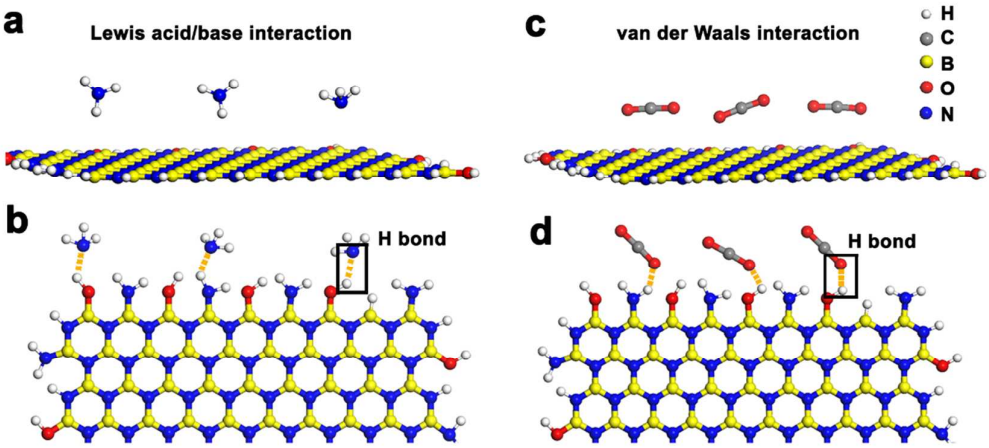


The adsorption mechanisms of $NH_3$ and $CO_2$ molecules on 3D FBNNSs